Flow Patterns and Comparison with Correlations for Vertical Flow Boiling of R245fa in Small to Micro Tubes

Tassos G. KARAYIANNIS [1,*], Emily A. PIKE-WILSON[1], Lejun CHEN [2], Mohamed MAHMOUD[1,3], Yongsheng TIAN[4]

* Corresponding author: tassos.karayiannis@brunel.ac.uk
1 School of Engineering and Design, Brunel University London, Uxbridge, UB8 3PH, UK
2 Sunrise Systems, Cambridge, CB25 9QZ, UK
3 Faculty of Engineering, Zagazig University, Zagazig, Egypt
4 British Energy, Gloucester, GL4 3RS, UK

Abstract Flow boiling patterns of R245fa in a 1.1 mm diameter copper tube were used to evaluate flow pattern maps in small to micro tubes. The flow boiling experiments were conducted over an experimental range of mass flux 100-400 kg/m^{2}s, heat flux 3-25 kW/m^2, inlet pressure of 1.85 and 2.45 bar and inlet subcooling of 5 K. The test section was heated directly using DC current. The effect of hysteresis was also investigated by increasing and decreasing the heat flux. A borosilicate glass observation section at the test section outlet was used for flow visualization. Hysteresis was evident across the whole experimental range, with obvious changes in the flow patterns between increasing and decreasing heat flux. The four main flow patterns were bubbly, slug, churn and annular flow. Confined flow was also evident. For increasing heat flux, only annular flow was evident but all the flow patterns were evident with decreasing heat flux. Therefore, the evaluation of flow pattern maps carried out in the present study was based on the decreasing heat flux data, as this covered the full range of flow patterns.

Keywords: Flow boiling, microtube, flow patterns correlations

1. Introduction

The application of flow boiling in microchannels is a constantly evolving research area, currently restricted by the limitations in heat transfer rates, pressure drop and flow pattern knowledge and the ability to accurately predict these factors. A recent review by Mahmoud et al. (2014) is available, which includes a section on past work on flow patterns in small to micro tubes. Flow pattern maps and prediction methods are available in literature but these are often restricted to particular experimental conditions and certain fluids. They mostly employ dimensionless numbers, based on the fluid properties and the channel diameter. No consideration is usually given to surface finish or channel material. Most of these flow pattern maps are plotted as a function of the superficial liquid and vapour velocities as seen in the work of Mishima and Hibiki (1996) and Yang and Sheih (2001) or the liquid and vapour Weber numbers reported in Akbar et al. (2003) and Chen et al. (2006). A limitation in the development of new flow pattern maps is the fact that the controlling forces responsible for flow pattern transitions are not fully understood.

Hassan et al. (2005) stated that many correlations available for predicting flow transitions are too specific and cannot be widely applied. Yang and Shieh (2001) conducted experiments with air-water and R134a, concluding that the fluid properties were a controlling variable in flow pattern transitions. For small diameter channels, the buoyancy force, turbulent fluctuations and the surface tension were all deemed important. For example, a larger surface tension force will delay the transition from slug to annular flow. R134a has a smaller surface tension than water. Hence for this refrigerant the transition from slug to annular transition occurs at lower gas velocities, which flow pattern maps may not predict. Shao et al. (2009) also concluded that flow pattern maps did not account for all

the parameters which affect the flow pattern transitions. The dominating factors for flow transitions were thought to be the channel size, superficial velocities, liquid phase surface tension and channel wettability. The development of future flow pattern maps requires a large databank of results with varying fluid properties and experimental conditions so that the dominating forces can be evaluated. This is currently hindered by the inconsistencies found in available data, even when using the same refrigerant and channel diameter. Karayiannis et al. (2012) suggested that these discrepancies were due to the surface characteristics and heated length. As indicated by Consolini et al. (2009), flow stability was also an important factor. A study by Mahmoud et al. (2011) into the effects of surface characteristics using seamless and welded stainless steel tubes found a difference in the heat flux value at the occurrence of the first bubbles (with the welded tube requiring a higher heat flux) and the trend in the heat transfer coefficient with quality or distance along the tube. However, in this study, the flow patterns for both tubes were similar. Further issues arise from contradictions in the method of defining the flow patterns. There are variances in both the flow patterns seen and the terminology used to define the flow patterns. Baldassari and Marengo (2013) noted that a possible reason for the discrepancies in flow pattern maps could be due to the difficulty in flow pattern identification in microchannels and the increasing relative errors with a decreasing diameter. Hassan et al. (2005) used a databank of 1475 points and found discrepancies in the reported flow patterns. From this, two universal flow pattern maps were produced, one for horizontal and one for vertical flow, which have set transition lines based on superficial velocities. Chen et al. (2006) studied the effect of tube diameter on flow patterns using R134a in 1.1-4.26 mm diameter tubes. This study identified flow patterns of dispersed bubble, bubbly, confined bubble, slug, churn, annular and mist flow. The confined flow, only seen for smaller diameter channels, is a point of contention with some researchers referring to this as slug flow. However, there is clear difference between confined flow and slug flow in the shape of the bubble tail. Confined flow has a rounded end as opposed to slug flow which has a disturbed end and can have a trail of bubbles. Many of the flow patterns in literature use a variation of these definitions, although often less detailed, e.g. no distinction between dispersed bubble and bubbly. Barnea et al. (1982) proposed a critical diameter, d_c, given in Eq. (1), to identify transition from dispersed bubble to bubbly flow when the bubbles tend to deform and coalesce easily.

$$d_c = 2\left[\frac{0.4\sigma}{(\rho_l - \rho_g)g}\right]^{1/2} \quad (1)$$

This diameter depends on the surface tension and the density difference of liquid and gas, which relate to pressure. Taitel (1990) supported the above and expected that the dispersed bubble flow would change to bubbly flow when the diameter of the bubbles is larger than the critical diameter. An alternative method of flow pattern categorization was presented by Ong and Thome (2011) who produced a flow pattern map based on the transitions from isolated bubble, coalescing bubble, slug-plug and annular flow regimes.

Experimental methodology

Experiments were conducted over a range of heat and mass fluxes, i.e. 3-25 kW/m^2 and 100-400 kg/m^2 s, for two inlet pressures of 1.85 and 2.45 bar using R245fa in a 1.1 mm diameter tube constructed of copper with vertical upward flow. The test facility was previously used to investigate the flow patterns of R134a. Details of this and the test facility can be found in Huo et al. (2004) and Mahmoud et al. (2014). The test section consists of a 150 mm calming section, to ensure fully developed flow and a pre-heater to control the inlet temperature. The copper test section is 300 mm long and heated directly using DC current with the supplied power being measured using a Yokogawa power meter WT110 with a manufacturer recorded

accuracy of ±0.29 %. The inlet and outlet temperatures are recorded using T-type thermocouples with an accuracy of ±0.18 K. Pressure transducers are used at these locations to record the pressure with an accuracy of ±1.5 %. The pressure drop across the heated section is recorded with a differential pressure transducer (PX771A-025DI) with a measuring accuracy of ±0.08 %. Fourteen equidistant K-type thermocouples are attached to the heated section using electrically insulating and thermally conducting epoxy, with a mean absolute error of ±0.23 K. Heat transfer and pressure drop data were recorded over a 90 second period, simultaneously as flow pattern data being recorded. Flow visualization is possible through a borosilicate glass tube, of 1.1 mm internal diameter, which is located at the heated section outlet. A high speed camera (Photo-Sonics Phantom V4B/W) records at 1000 frames per second with a resolution of 512 x 512 pixels. Data is recorded when the test facility is deemed to be in a steady state based on oscillations in the mass flow rate, pressure and temperatures at the inlet, see Karayiannis et al. (2012).

Results and discussion

The flow patterns in small to micro diameter tubes are commonly defined as bubbly, confined bubble, slug, churn and annular flow. Note that in the work of Chen et al. (2006) for R134a, in stainless steel tubes with diameters ranging from 1.1 mm to 4.26 mm, very clear photographs of dispersed bubble flow were observed. In this regime, the bubbles were more in number and smaller than what were referred to in Chen et al. and here in this paper as bubbly flow. In the present study, the flow patterns for an increasing heat flux are limited to some occurrence of slug and churn flow and a dominance of annular flow. However all the above flow patterns (bubbly, confined bubble, slug, churn and annular flow) were observed with decreasing heat flux. Therefore, the comparison with flow pattern maps is based on the decreasing heat flux results. The difference in flow patterns seen for increasing and decreasing heat fluxes is thought to be as a result of hysteresis. Nucleation site activation is related to the wall superheat, with smaller cavities requiring a larger wall superheat to be activated. The wall superheat is higher with increasing heat flux than for decreasing heat flux. This higher wall superheat should allow for small nucleation sites to be activated with increasing heat flux. These can remain active when the heat flux is then decreased, resulting in flow patterns which were not seen for increasing heat flux. For all mass fluxes, annular flow was the dominant flow pattern. Figure 1 presents the flow patterns at a mass flux of 200 kg/m^{2}s. Pike-Wilson and Karayiannis (2014) reported experiments with tubes made of three materials, namely stainless steel, brass and copper (present tube) all with a diameter of 1.1 mm. The flow patterns of Fig. 1 were evident for all three tubes with a decreasing heat flux but at different exit qualities and heat fluxes, which indicates some effect of surface characteristics.

Bubbly	Confined bubble	Slug	Churn	Annular
x_e= 0.008	x_e= 0.017	x_e= 0.054	x_e= 0.099	x_e= 0.14
q=1.1	q=2.0	q=3.3	q=4.6	q=6.7 kW/m^2

Fig. 1. Flow patterns at G=200 kg/m^{2}s and P=1.85 bar with a decreasing heat flux.

Flow pattern maps

The flow patterns were recorded for the two inlet pressures, 1.85 and 2.45 bar, with no major differences in the flow transitions. The comparisons that follow are made based on an inlet pressure of 1.85 bar. Figure 2 presents a comparison of the present flow patterns with the predictions of the vertical flow pattern map of Hassan et al. (2005) based on superficial velocities. In Hassan et al. the intermittent region includes confined bubble and slug flow. This map covers a larger range of superficial gas and liquid velocities than seen with the experimental data. The annular flow transition is predicted moderately well, with the prediction improving with the mass flux. The bubbly and slug flow are predicted to occur at a lower superficial gas velocity than seen experimentally.

A comparison of the flow patterns is also conducted based on the liquid and vapour Weber numbers, suggested by Chen et al. (2006) who concluded that the Weber number was useful for incorporating the effects of surface tension and inertia forces. Figure 3 presents the Weber number plot from Chen et al. (2006) using R134a, where the flow transitions are clearly visible. Note that the range of Weber number for R245fa for similar experimental conditions will be different due to differences in surface tension, liquid density and vapour density between the two fluids.

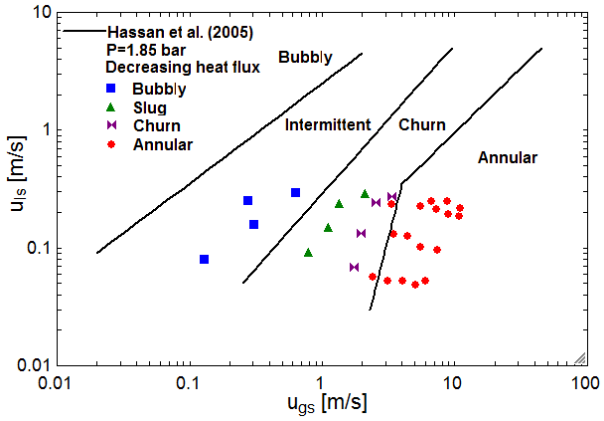

Fig. 2. Comparison of experimental data with Hassan et al. (2005).

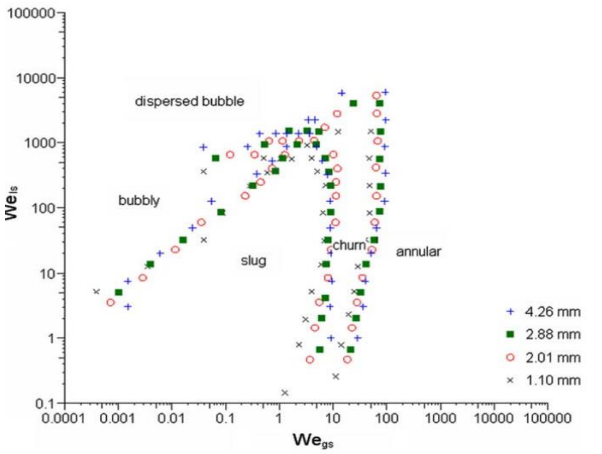

Fig. 3. Experimental results for R134a and different diameters, at 6 bar, Chen et al. (2006).

Chen (2006) produced a detailed map based on the liquid and vapour superficial velocities with flow pattern transitions calculated based on the refrigerant properties and experimental data covering upward flow of R134a, inlet pressures 6, 10 and 14 bar and corresponding vapour quality and mass flux ranges of 0.05% - 90% and 50-6400 kg/m^{2}s, see Fig. 4 for 2.01 mm tube at 10 bar as an example. Chen used the same experimental facility as the present work and stainless steel tubes of diameters 4.26, 2.88, 2.01 and 1.1 mm. The flow patterns were viewed at the same location as described in this paper, through the borosilicate glass tube located at the exit of the heated test section.

Chen gave the following equations that describe the transition lines of the flow map shown in Fig. 4:

Churn-annular transition boundary: this boundary was described using two equations; Eq. (2) for line A and Eq. (3) for line B.

$$We_{ls} = 1.567\times10^{-17}\left(Fr_{gs}\,\mathrm{Re}_{gs}\right)^{3.41} \qquad (2)$$

$$Fr_{gs}\,\mathrm{Re}_{gs} = 3.119\times10^{5} \qquad (3)$$

Slug-churn transition boundary: this boundary was described using three equations namely Eq. (4) for line G, Eq. (5) for line H and Eq. (6) for line I as given below:

$$\mathrm{Re}_{ls} = 81.08 We_{gs}^{1.626} Fr_{\mathrm{gs}}^{*\,-0.267} \quad (4)$$

$$u_{gs} = 587.1 \left(\frac{\mu_l}{\rho_g D} \right)^{1.447} \left(\frac{\rho_g D}{\sigma} \right)^{0.937} \quad (5)$$

$$u_h = 2.75 \sqrt{\frac{\sigma}{f_l \rho_l D}} \quad (6)$$

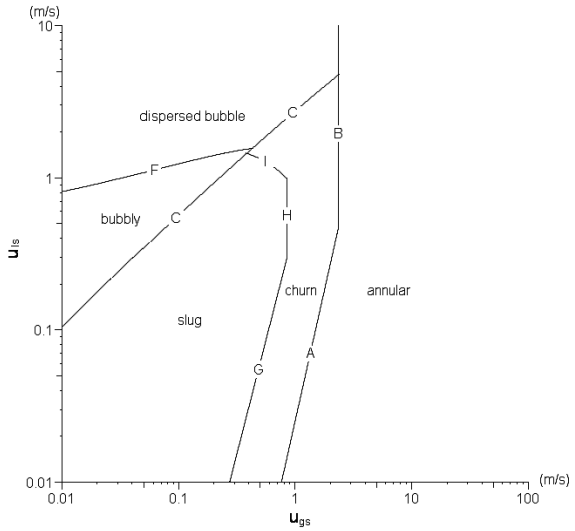

Fig. 4. Flow pattern transition boundaries defined in Chen (2006) for *D* = 2.01 mm and *P* = 10 bar.

Chen (2006) stated that this transition boundary occurs due to three different mechanisms. The first is bubble elongation which occurs at low liquid superficial velocity (line G). At a certain bubble length the bubble starts to distort. The second is the deformation of the slug nose and tail due to the presence of chaotic flow field in the tail region at an intermediate liquid superficial velocity range (line H). The third mechanism occurs at high liquid superficial velocity (line I) where the bubble cannot keep its regular shape due to the dominance of turbulence over surface tension force. Accordingly, the fanning friction factor f_l in Eq. (6) is calculated based on turbulent flow and the homogeneous Reynolds number as given by Eq. (7) which is cited in Jayanti and Hewitt (1992).

$$f_l = 0.046 \,\mathrm{Re}_h^{-0.2} \quad (7)$$

Bubbly-slug and dispersed bubble-churn transition boundaries: this boundary (line C) was proposed to occur when the void fraction α in Eq. (8) equals a critical value (α_c). Some researchers found that the void fraction at which bubbly-slug and dispersed bubble-churn transition occurs does not depend on experimental conditions. For example, Taitel (1990) found that the critical void fraction value is 0.25 for bubbly-slug transition and 0.52 for dispersed bubble-churn transition. Contrary to that, Chen found that the critical void fraction depends on experimental conditions (diameter, pressure, fluid properties). As a result, he gave a correlation for the critical void fraction, see Eq. (9).

$$u_{ls} = \left(\frac{1}{\alpha C_0} - 1 \right) u_{gs} - \frac{u_d}{C_0} \quad (8)$$

$$\alpha_c = c_1 \left(u_{gs} + u_{ls} \right)^{c_2} \quad (9)$$

Chen (2006) plotted the measured void fraction at which transition occurs versus the homogeneous velocity ($u_{gs} + u_{ls}$) and fitted the data to get c_1 and c_2. The values of these constants were found to be $c_1 = 0.138$ and $c_2 = 0.344$. The void fraction was measured from the pictures recorded by the high speed camera. In each picture, the number of bubbles and the average bubble diameter were determined. Thus, the volumetric void fraction was calculated as the ratio of the total gas volume to the mixture volume. Chen (2006) did not propose a correlation for the distribution parameter and the drift velocity in Eq. (8). Instead, he used his measured values which depend on pressure and diameter. Thus, Eqs. (10) and (11) cited in Mishima and Ishii (1996) are recommended by the present authors to generalise this model. It is worth mentioning that Eq. (9) is valid for both dispersed bubble-churn and bubbly-slug transition boundaries as reported by Chen (2006).

$$C_0 = 1.2 - 0.2 \sqrt{\rho_g / \rho_l} \quad (10)$$

$$u_d = 0.35 \sqrt{gD(\rho_l - \rho_g)/\rho_l} \quad (11)$$

Dispersed bubble-bubbly transition boundary: this boundary (line F) is given by Eq. (12) and is not included in the present comparison, i.e. no dispersed flow was reported.

$$u_l = 0.45\left[1+4\left(\alpha_{act} We_b^{1/2}\right)^{1/3}\right]\left(\frac{\sigma}{f_l \rho_l d_c}\right)^{1/2} \quad (12)$$

Since the actual measured void fraction (α_{act}) was found to be less than the calculated one ($\alpha_{cal} = u_{gs}/(u_{gs}+u_{ls})$), a correction factor K such that $\alpha_{act} = K\alpha_{cal}$ is recommended by Chen (2006). As a result, the liquid velocity u_l was given by Eq. (13) and the values of K are summarized in Table (1).

$$u_l = \frac{(\rho_g u_{gs} + \rho_l u_{ls})(u_{gs}+u_{ls})}{K(\rho_g u_{gs} - \rho_l u_{gs}) + \rho_l (u_{gs}+u_{ls})} \quad (13)$$

Again, due to the fact that this transition boundary occurs at high liquid velocity, turbulent condition is dominating. Therefore, f_l in Eq. (12) is calculated as discussed above using Eq. (7).

Table 1 The correction coefficient K for the void fraction for R134a.

D = 1.1 mm			
P [bar]	6	10	14
K	0.212	0.24	0.296
D = 2.01 mm			
P [bar]	6	10	14
K	0.4	0.604	0.625
D = 2.88 mm			
P [bar]	6	10	14
K	0.181	0.371	0.624
D = 4.26 mm			
P [bar]	6	10	14
K	0.299	0.391	0.562

The general applicability of Eq. (12) for flow boiling needs to be considered further since the K factors proposed are based on R134a data only.

Figure 5 compares the transition boundaries calculated from the equations above (obtained from R134a data) and compares these with the present results for R245fa. Note that Eq. (12) is not included as we did not observe dispersed flow for R245fa in the present experimental conditions. This flow pattern map showed an improvement from the Hassan et al. (2005) model depicted in Fig. 2. The slug, churn and annular flow patterns are predicted very well. On the contrary, the bubbly-slug transition boundary exhibited high deviation compared to the experimental values, where bubbly flow is predicted to occur at a much higher liquid superficial velocities. This may be attributed to the fact that bubbly flow in the current study occurred only due to nucleation sites hysteresis when the heat flux was decreased, which was not the case in the study of Chen (2006). This hysteresis is arising from the difference in surface characteristics (copper in the present study versus stainless steel in the Chen study). A comparison of Figs. 2 and 5 shows a similarity in the predicted annular transition at lower superficial liquid velocities. Also, it is worth noting that, the predicted transition for bubbly flow shows a similar gradient and deviation as the prediction by Hassan et al. (2005).

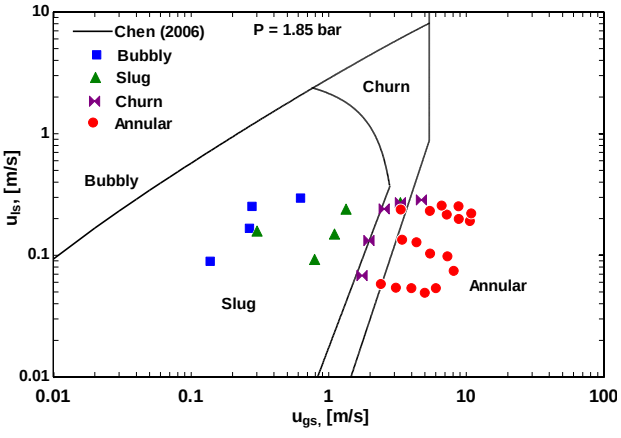

Fig. 5. Comparison of experimental flow patterns for R245fa at 1.85 bar with the predictions of the equations given in this paper from Chen (2006).

As previously discussed, Chen (2006) reported three different mechanisms for the

transition from slug to churn, see Eqs. (4-6) which are corresponding to lines *G*, *H* and *I* in Fig. 4. Inspecting Fig. 5, one can see that the slug-churn transition boundary is only represented by lines *G* and *I* while line *H* is not included which needs a comment. According to Fig. 4 for R134a, line *I* intersects with line *H* at high liquid superficial velocity, which is greater than that at the intersection of line *G* with line *H*. On the contrary, for R245fa, line *I* was found to intersect with line *H* at very low liquid superficial velocity which crosses the annular region. This means that the slug-churn mechanism corresponding to line *H* (disturbance at the tail of the slugs) seems to diminish for this fluid. Figure 1 may support this point where no chaotic disturbance at the tail of the slugs was observed. In other words, the other two mechanisms (line *G* and *I*) are dominating. Inspecting Eqs. (4-6) one can see that these mechanisms depend on fluid properties. This transition boundary needs to be studied further due to the effect of fluid on the most dominant transition mechanism.

An alternative flow pattern map is that of Ong and Thome (2011) shown in Fig. 6 in terms of mass flux and vapour quality. The flow transition boundaries are based on dimensionless numbers, which include refrigerant properties and experimental data for R134a, R236fa and R245fa. The flow pattern definitions differ from those used in this study. Ong and Thome defined their flows as isolated bubble (IB), slug-plug (P-S), coalescence bubble (CB) and annular flow. As seen in the comparison of the figure, the transition from IB to P-S and CB, which could correspond to transition from bubbly to slug flow is predicted reasonably well. However, the model predicts a high vapour quality for a given mass flux for the transition to annular flow compared to the present results. The slug-plug regime is predicted to occur only at lower mass fluxes and consequently the slug flow presence is not predicted well.

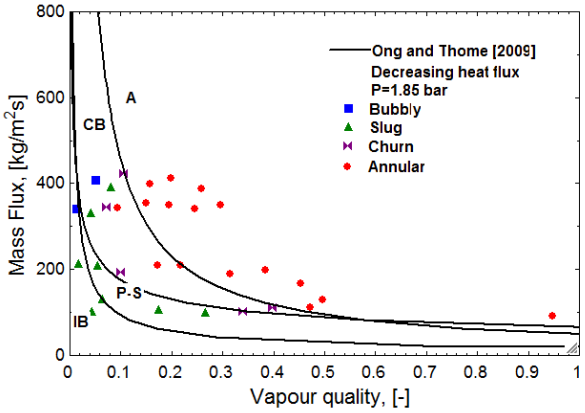

Fig. 6. Comparison of experimental data with Ong and Thome (2011) model for a pressure of 1.85 bar.

Costa-Patry et al. (2012) produced a heat transfer prediction method based on flow patterns. This model is based on a modified Thome et al. (2004) model for the intermittent flow (IB-CB transition) and a modified Cioncolini and Thome (2011) model for the annular flow. Figure 7 presents the flow transitions from the Costa-Patry et al. model compared with the experimental data. This model shows improved prediction for the transition to annular flow compared to the Ong and Thome (2011) model at lower mass fluxes but reduced accuracy for churn flow occurrence.

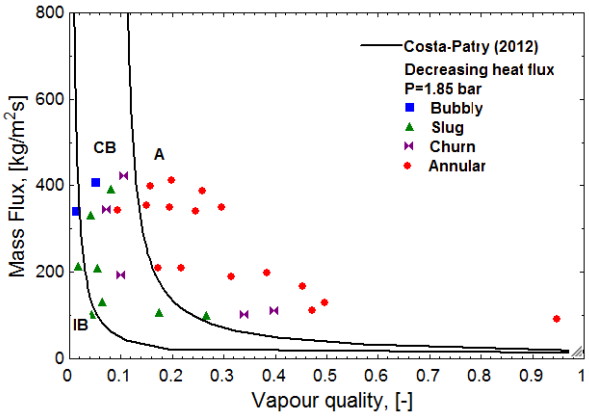

Fig. 7. Comparison of the experimental flow pattern data with the Costa-Patry et al. (2012) model.

Conclusions

Flow patterns were recorded in a 1.1 mm diameter vertical tube made of copper at inlet pressures of 1.85 and 2.45 bar, mass flux ranging from 100 to 400 kg/m^{2}s and both increasing and decreasing heat flux in the range of 3 to 25 kW/m^2. The resulting flow patterns were identified as bubbly, confined bubble, slug, churn and annular flow. The flow patterns were seen to vary for increasing and decreasing heat fluxes. For increasing heat flux we observed some occurrence of slug and churn flow but a dominance of annular flow. All the above mentioned flow patterns (bubbly, confined bubble, slug, churn and annular) were seen with decreasing heat flux. This clear effect of increasing and decreasing heat flux on flow patterns is not widely discussed in literature and may explain differences in reported flow pattern data given by various research groups. Annular flow occurred at lower superficial gas velocities and vapour qualities than predicted by some of the models. The flow pattern map described in the paper based on equations (1-13) predicted the majority of the flow transition boundaries fairly well except the transition from bubbly to slug. Hysteresis effects may account to this difference. Further research is needed and recommended to evaluate and validate this proposed map, including some of the empirical constants used, for different operating ranges, fluids and passage geometries.

Acknowledgements

E. Pike-Wilson would like to acknowledge and thank the Thomas Gerald Grey Charitable Trust for providing a scholarship during her studies at Brunel University London.

Nomenclature

C_0	distribution parameter
c_1	experimental coefficient for critical void fraction on bubbly slug boundary, Eq. (9)
c_2	experimental exponent for critical void fraction on bubbly-slug boundary, Eq. (9)
D	tube diameter (m)
d_c	critical bubble diameter, Eq (1) (m)
Fr_{gs}	Froude number based on gas superficial velocity, $Fr_{gs} = u_{gs} / \sqrt{gD}$
Fr^*_{gs}	modified Froude number based on gas superficial velocity, $Fr^*_{gs} = u_{gs}\sqrt{\rho_g /(\rho_l - \rho_g)gD}$
f_l	friction factor based on homogeneous velocity.
g	gravitational acceleration (m/s^2)
P	pressure (Pa)
q	heat flux (W/m^2)
Re_{gs}	Reynolds number based on gas superficial velocity, $\mathrm{Re}_{gs} = \rho_g u_{gs} D / \mu_g$
Re_h	Reynolds number based on homogeneous velocity, $\mathrm{Re}_h = \rho_l u_h D / \mu_l$
Re_{ls}	Reynolds number based on liquid superficial velocity, $\mathrm{Re}_{ls} = \rho_l u_{ls} D / \mu_l$
u_d	drift velocity, (m/s)
u_{gs}	gas superficial velocity (m/s)
u_h	homogeneous velocity (m/s), $u_h = u_{gs} + u_{ls}$
u_l	liquid velocity defined by Eq. (13)
u_{ls}	liquid superficial velocity (m/s)
We_b	Weber number based on bubble diameter and homogeneous velocity, $We_b = \rho_g u_h^2 d_c / \sigma$
We_{gs}	Weber number based on gas superficial velocity, $We_{gs} = \rho_g u_{gs}^2 D / \sigma$
We_{ls}	Weber number based on liquid superficial velocity, $We_{ls} = \rho_l u_{ls}^2 D / \sigma$
x_e	exit vapour quality, (-)

Greek symbols

α	void fraction
α_{act}	actual void fraction
α_{cal}	calculated void fraction, $u_{gs}/(u_{gs} + u_{ls})$
α_c	critical void fraction
μ_g	gas dynamic viscosity (kg/m.s)

μ_l liquid dynamic viscosity (kg/m.s)
ρ_g gas density (kg/m^3)
ρ_l liquid density (kg/m^3)
σ surface tension (N/m)

References

Akbar, M.K., Plummer, D.A., Ghiaasiaan, S.M., 2003. On gas-liquid two-phase flow regimes in microchannels, Int. J. Mulitphase Flow, 29: 855-865.

Baldassari, C., Marengo, M., 2013. Flow boiling in microchannels and microgravity, Progress in Energy and Combustion Science, 39 (1): 1-36.

Barnea, D., Shoham, O. and Taitel, Y., 1982. Flow pattern transition for vertical downward two-phase flow, Chemical Engineering Science, 37: 741-746.

Chen, L., Tian, Y.S., Karayiannis, T.G., 2006. The effect of tube diameter on vertical two-phase flow regimes in small tubes, Int. J. Heat Mass Transfer, 49 (21-22): 4220-4230.

Chen, L., 2006, Flow patterns in upward two-phase flow in small diameter tubes, PhD thesis, Brunel University London, UK.

Consolini, L., Thome, J.R., 2009. Micro-channel flow boiling heat transfer of R134a, R236fa and R245fa. Microfluidics and Nanofluidics, 6: 731-746.

Cioncolini, L., Thome, J.R., 2011. Algebraic turbulence modelling in adiabatic and evaporating annular two phase flow, Int. J. of Heat and Fluid flow, 32,805-817.

Costa-Patry, E., Olivier, J., Thome, J.R., 2012. Heat transfer characteristics in a copper micro-evaporator and flow pattern-based prediction method for flow boiling in microchannels, Frontiers in Heat and Mass Transfer, 3.

Huo, X., Chen, L, Tian, Y.S., Karayiannis, T.G., 2004. Flow boiling and flow regimes in small diameter tubes, Applied Thermal Engineering, 24: 1225-1239.

Hassan, I., Vaillancourt, M., Pehlivan, K., 2005. Two-phase flow regime transitions in microchannels: A comparative experiemental study, Microscale Thermophysical Engineering, 9(2):165-182.

Jayanti, S. and Hewitt, G. F., (1992). Prediction of the slug-to-churn flow transition in vertical two phase flow. Int. J. Multiphase Flow, 18(6): 847-860.

Karayiannis, T.G., Mahmoud, M.M., Kenning, D.B.R., 2012. A study of discrepancies in flow boiling results in small to microdiameter metallic tubes, Exp. Thermal and Fluid Sci. 36: 126-142.

Mahmoud, M.M., Karayiannis, T.G., Kenning, D.B.R., 2011. Surface effects in flow boiling of R134a in microtubes, Int. J. Heat Mass Transfer, 54, 3334-3346.

Mahmoud, M.M., Karayiannis, T.G., Kenning, D.B.R., 2014. Flow boiling in small to microdiameter tubes, Chapter 10, Emerging Topics in Heat Transfer Enhancement and Heat Exchangers, 321-396, WIT Press.

Mishima, K., Hibiki, T., 1996, Some characteristics of air-water two-phase flow in small diameter vertical tubes, Int. J. of Multiphase Flow, 22: 703-712.

Ong, C.L., Thome, J.R., 2011. Macro-to-microchannel transition in two-phase flow: Part 1- Two phase flow patterns and film thickness measurements, Exp. Thermal and Fluid Sci. 35: 37-47.

Pike-Wilson, E., Karayiannis, T.G., (2014) Flow boiling of R245fa in 1.1 mm diameter stainless steel, bras and copper tubes. Exp. Thermal and Fluid Sci., http://dx.doi.org/10.1016/j.exptherflusci.2014.02.0242014.

Shao, N., Gavriilidis, A., Angeli, P., 2009. Flow regimes for adiabatic gas-liquid flow in microchannels, Chemical Engineering Science, 64: 2749-2761.

Taitel, Y., 1990. Flow pattern transition in two phase flow, 9th International Heat Transfer Conference, Jerusalem, Israel, 19-24 Aug., 237-254.

Thome, J.R., Dupont, V., Jacobi, A., 2004. Heat transfer model for evaporation in microchannels. Part I: Presentation of the model, I J of Heat and Mass transfer, 47: 3387-3401.

Yang, C.Y., Shieh, C.C., 2001. Flow pattern of air-water and two-phase R134a in small circular tubes. Int. J. Mulitphase Flow, 27: 1163-1177.